Macromolecules

Article

pubs.acs.org/Macromolecules

High Performance Graded Rainbow Holograms via Two-Stage Sequential Orthogonal Thiol–Click Chemistry

Haiyan Peng,[†,‡] Devatha P. Nair,[†] Benjamin A. Kowalski,[§] Weixian Xi,[†] Tao Gong,[†] Chen Wang,[†] Michael Cole,[§] Neil B. Cramer,[†] Xiaolin Xie,[‡] Robert R. McLeod,[§] and Christopher N. Bowman*[,†]

[†]Department of Chemical and Biological Engineering, University of Colorado, UCB 596, Boulder, Colorado 80309, United States
[‡]School of Chemistry and Chemical Engineering, Huazhong University of Science and Technology, Wuhan 430074, China
[§]Department of Electrical, Computer and Energy Engineering, University of Colorado, Boulder, Colorado 80309, United States

Supporting Information

ABSTRACT: Orthogonal, sequential "click" reactions were implemented to yield novel polymeric substrates with the ability to record holographic data. The base-catalyzed thiol–acrylate Michael "click" reaction was implemented to yield a writable, stage 1 polymeric substrate with glass transition temperatures (T_g) ranging from 0 to −26 °C and rubbery storage moduli (E') from 11.1 to 0.3 MPa. The loosely cross-linked matrix also contained a novel high refractive index monomer 9-(2,3-bis(allyloxy)propyl)-9*H*-carbazole (BAPC) that did not participate in the thiol–Michael reaction but allowed for large index gradients to be developed within the network upon subsequent exposure to coherent laser beams and initiation of the radical-mediated thiol–ene reaction. The holographic gratings were recorded with 96% diffraction efficiency and ca. 2.4 cm/mJ of light sensitivity in 2 s under a 405 nm exposure with an intensity of 20 mW/cm^2. Subsequent to pattern formation, via a thiol–allyl radical "click" photopolymerization initiated by flood illumination of the sample, holographic materials with high T_g, high modulus, diffraction efficiency as high as 82%, and refractive index modulation of 0.004 were obtained. Graded rainbow holograms that displayed colors from blue to red at a single viewing angle were readily formed through this new technique.

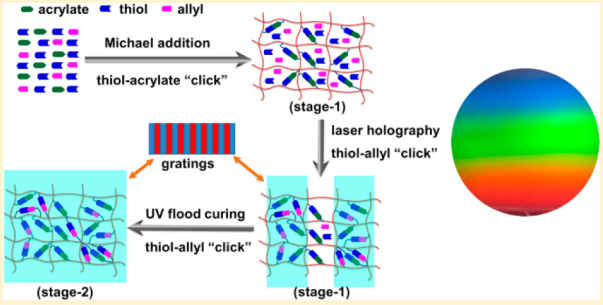

1. INTRODUCTION

Holograms, generated from the interference of multiple coherent laser beams, are of immense utility in a myriad of applications such as data storage,[1−4] anticounterfeiting systems,[5] holographic optical elements,[6] and colorful 3D displays.[7−9] Bragg (that is, thick) holograms cannot generally utilize solvent processing and are sensitive to dimensional changes, which has led to the development of several elegant substrates with reactive monomers embedded in a solid network,[10−14] where these reactive monomers polymerize selectively during holographic illumination to result in refractive index gradients. However, most holograms are generated based on the chain-growth polymerization mechanism, which are generally oxygen sensitive and thus need protective layers to minimize the oxygen inhibition. Yet, the presence of a protective layer can cause unexpected gratings and grating distortions within the substrate; additionally, the light sensitivity (<0.5 cm/mJ) of many current techniques are too low, resulting in these photopolymers often being susceptible to undesirable ambient variations or thermal expansion, particularly when large size holograms are recorded, even when fully enclosed air damped optical tables are used.[6] Thus, there are considerable challenges and opportunities to enhance current photopolymer substrates by increasing the light sensitivity and oxygen tolerance of the holographic substrates. In this study we utilize the orthogonal "click" reaction paradigm and combine the inherent advantages of thiol–click chemistry to formulate holographic substrates.

Orthogonal click reactions, sequentially or simultaneously involving at least two "click" pathways, have provoked a great deal of interest ascribed to the synergistic advantages that include high chemical selectivity, high functional group tolerance, regioselectivity and stereospecificity, rapid kinetics, mild conditions, insensitivity to oxygen or water, quantitative conversion, and absence of byproducts or side reactions.[15−18] Chan and co-workers were one of the first to implement the sequential thiol–Michael/thiol–yne click reactions to form polyfunctional materials.[19] Anseth and co-workers formulated hydrogels for encapsulating cells in three-dimensional microenvironments though strain-promoted azide–alkyne click reactions which were then subjected to biochemical patterning via thiol–ene radical coupling.[16,20] Azide–alkyne/thiol–ene orthogonal click reactions have also been utilized to form microarrays,[21] amphiphiles,[22] and Janus particles.[23] Similarly,

Received: January 21, 2014
Revised: March 14, 2014
Published: March 28, 2014

Scheme 1. (a) Schematic Illustration of Holography through Two-Stage Orthogonal Thiol−Click Chemistry and (b) the Monomers Used in This Study

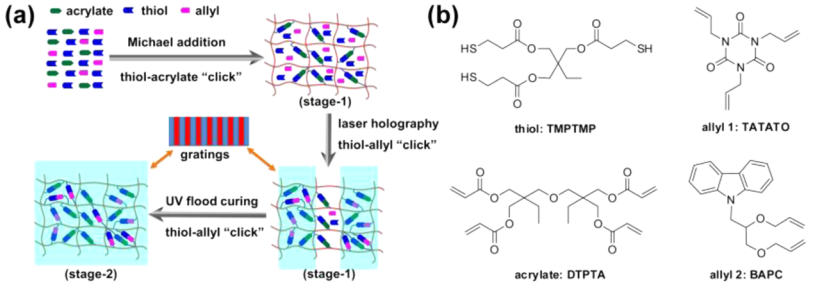

Scheme 2. Mechanisms for (a) Base-Catalyzed Thiol−Michael Addition and (b) Radical-Mediated Thiol−Ene Polymerization within the Two-Stage Reactive Polymer Paradigm[38,49]

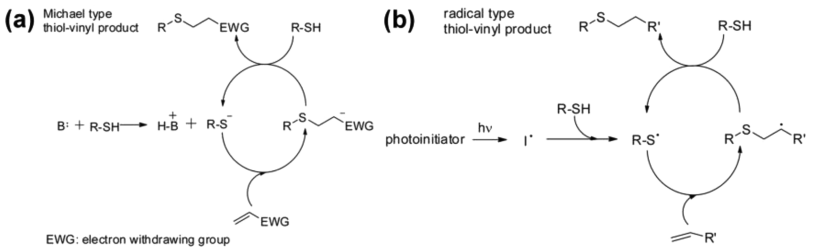

hyperbranched polymers were prepared through thiol−yne and sequential azide−alkyne click reactions.[24,25] The innovation of phototriggered azide−alkyne cycloaddition affords these orthogonal click protocols more methodologies of temporally and spatially controlling reactions and extending applications.[26−29] Other extensive orthogonal click techniques for polymer synthesis and functionalization have also been developed.[30−36] Thus, as the exploration of orthogonal click chemistry in synthesis and bioengineering realms continues to evolve, its implementation in other areas of materials science remains relatively limited. Herein, we implement this powerful paradigm in novel holographic substrate formulations to yield holograms with good fidelity and light sensitivity.

Thiol−ene click chemistries can be implemented via the radical-mediated step-growth mechanism. In addition to the advantages of a traditional click reaction such as the ability to be easily implemented under mild and neat conditions, the capability to form ideal, uniform, and homogeneous polymer networks with narrow glass transition peak,[15,37−40] the nature of the radical-mediated thiol−ene reaction makes it amenable to both temporal and spatial control, making it ideal for complex stereolithography[34] or 4D tissue engineering applications.[20,41] Compared to chain-growth polymerizations, the thiol−ene step-growth reaction exhibits 35−48% lower volumetric shrinkage (12−15 mL/mol C═C), much higher gel point conversions of the double bonds, and better oxygen tolerance.[37,42] The advantages offered by the thiol−ene reactions in formulating polymer holograms have been explored. By loading 35 vol % of nanoparticles in thiol−ene mixtures, Tomita and co-workers obtained as low as 0.3% of polymerization volume shrinkage and as high as 0.008 of index modulation during holography.[43] The Bunning and Guymon groups have also obtained high performance holographic polymer dispersed liquid crystal (HPDLC) gratings through thiol−ene reactions.[44−46] Besides the traditional, radical-meditated anti-Markovnikov thiol−ene route, there are several alternate methods to mediate various thiol−click reactions.[37,38,40] For instance, thiol groups are also able to react with electron-deficient vinyl monomers through the well-known Michael addition which can be either base-[47,48] or nucleophile-catalyzed.[48,49] Working with the orthogonal nature of the thiol−Michael pathway to other radical pathways, recently Nair et al. explored a two-stage approach for designing materials such as dual-cure shape memory polymers, impression materials, and holographic photoresists in which unreacted double bonds were embedded within the thiol−acrylate Michael addition networks.[50] The residual, unreacted functional groups were then reacted via exposure to light through a radical chain growth mechanism. This novel strategy afforded two distinct polymers with distinct material properties that enabled both the material handling and processing of the intermediate polymer as well as the ability to dial in the ultimate polymer properties. On the basis of this elegant two-stage method, Kloxin and co-workers[51] also demonstrated the photodirected formation and control of wrinkles within a two-stage reactive polymer.

By combining the two-stage and orthogonal click chemistry advantages, herein, we propose a novel strategy to develop holograms with high fidelity and high modulus based on a two-stage sequential orthogonal thiol−click polymerization technique (Scheme 1) in which through an initial thiol−acrylate Michael click reaction a photopolymeric substrate is developed with excess thiol−allyl reacting species embedded within this intermediate, loosely cross-linked network (i.e., a stage 1 polymer network). This proposal is based on the fact that the thiol−Michael addition and thiol−allyl radical polymerization proceed via orthogonal paths, since vinyl monomers without an electron withdrawing group conjugated with the C═C bond are incapable of participating in the Michael addition reaction while those with electron-deficient enes readily and rapidly react with the thiolate anions[37,48,49] (Scheme 2). By carefully and precisely controlling the stoichiometric ratio of the thiol, acrylate, and allyl monomers present within the network, the system is designed with a low T_g and modulus to optimize

dx.doi.org/10.1021/ma500167x | Macromolecules 2014, 47, 2306−2315

diffusion and reaction rates as required for holographic recording in stage 1 (i.e., writing step). Once diffusion during the holographic patterning within the cross-linked network has completed, the polymer network is subsequently flood cured by UV light, thereby reacting the excess thiol and allyl functional groups within the polymer network and resulting in a high modulus and T_g material with holographic fringes captured within the substrate (i.e., stage 2). Additionally, a high refractive index diallyl monomer, 9-(2,3-bis(allyloxy)propyl)-9*H*-carbazole (BAPC), that only participates in the thiol−ene reaction is added to afford high index modulation within this novel substrate.

2. MATERIALS AND EXPERIMENTAL SECTION

2.1. Materials. Carbazole (purity 96%) and glycidol (2,3-epoxy-1-propanol, purity 96%) were provided by Acros Organics. Allyl bromide (purity 97%), sodium hydride (purity 95%), di(trimethylolpropane)-tetraacrylate (DTPTA, $n_{20\ °C}$ = 1.479), and 1,3,5-triallyl-1,3,5-triazine-2,4,6(1*H*,3*H*,5*H*)-trione (TATATO, $n_{20\ °C}$ = 1.513, purity 98%) were obtained from Aldrich. Trimethylolpropane tris(3-mercaptopropionate) (TMPTMP) was donated by Evans Chemetics (Waterloo, NY). Aluminum *N*-nitrosophenylhydroxylamine (Q1301) was donated by Wako Pure Chemical (Osaka, Japan). 2,4,6-Trimethylbenzoyldiphenylphosphine oxide (TPO, purity 97%) was received from BASF Corporation. Triethylamine (TEA, purity ≥98%) was purchased from Fluka.

2.2. Synthesis and Characterization of 9-(2,3-Bis(allyloxy)-propyl)-9*H*-carbazole (BAPC). *Synthesis and Characterization of 3-(9H-carbazol-9-yl)propane-1,2-diol.* 50.3 g of carbazole, 25.9 g of KOH, and 150 mL of DMSO were added in a 250 mL dry round-bottom flask and stirred for 30 min at 80 °C, then added 30 mL of glycol dropwise, and kept stirring overnight. The mixture was quenched with 200 mL of DI water, and 1 M HCl was added until the pH dropped to 7. The organic phase was extracted by 400 mL of ethyl acetate, washed with 30 mL of brine, and then dried with anhydrous Na_2SO_4. The crude product was purified by silica gel column chromatography using hexane:EtOAc (4:1 in volume) to give a pure product (28 g, 38%) as a light red solid. ^{1}H NMR (Bruker Avance-III 400 spectrometer, 400 MHz, chloroform-*d*) δ: 8.10 (dt, J = 7.8, 1.0 Hz, 2H), 7.53−7.44 (m, 4H), 7.27 (d, J = 2.1 Hz, 1H), 7.25 (dd, J = 6.1, 2.1 Hz, 1H), 4.44 (dd, J = 6.5, 0.9 Hz, 2H), 4.28 (ddd, J = 6.3, 3.2, 2.1 Hz, 1H), 3.81−3.56 (m, 2H), 2.98 (d, J = 0.4 Hz, 1H).

Synthesis and Characterization of 9-(2,3-Bis(allyloxy)propyl)-9H-carbazole (BAPC). 9.0 g of 3-(9*H*-carbazol-9-yl)propane-1,2-diol, 2.7 g of sodium hydride, and 50 mL of THF were added to a 100 mL dried round-bottom flask, which was stirred for 30 min at room temperature; then 12.3 mL of allyl bromide was added dropwise and kept stirring overnight. The mixture was quenched by adding 10 mL of methanol and 50 mL of DI water. The organic phase was extracted by 100 mL of ethyl acetate, washed with 10 mL of brine, and then dried with anhydrous Na_2SO_4. The crude product was purified by silica gel column chromatography using hexane:EtOAc (5:1 in volume) to give a pure product (11 g, 92%) as light yellow liquid. ^{1}H NMR (Bruker Avance-III 400 spectrometer, 400 MHz, chloroform-*d*) δ: 8.09 (ddd, J = 7.8, 1.2, 0.7 Hz, 2H), 7.52 (dt, J = 8.3, 0.9 Hz, 2H), 7.45 (ddd, J = 8.2, 7.0, 1.2 Hz, 2H), 7.24 (ddd, J = 7.9, 7.0, 1.1 Hz, 2H), 5.95 (ddt, J = 17.2, 10.4, 5.6 Hz, 1H), 5.69 (ddt, J = 17.2, 10.3, 5.7 Hz, 1H), 5.35−5.17 (m, 2H), 5.13−4.99 (m, 2H), 4.63−4.34 (m, 2H), 4.05−3.80 (m, 5H), 3.57−3.36 (m, 2H). ^{13}C NMR (Bruker Avance-III 400 spectrometer, 101 MHz, $CDCl_3$) δ: 140.84, 134.63, 134.57, 125.67, 122.97, 120.20, 119.07, 117.26, 117.23, 109.29, 76.42, 72.46, 71.61, 69.47, 44.78. HRMS (PE SCIEX/ABI API QSTAR Pulsar Hybrid LC/MS/MS, ESI) calculated for $[C_{21}H_{23}NO_2]^+$($[MH]^+$): m/z 322.1807; found: 322.1807. The refractive index of BAPC was measured as ∼1.61.[52]

2.3. Real-Time Fourier Transform Infrared Spectroscopy (RT-FTIR). RT-FTIR was conducted on a Nicolet 750 Magna FT-IR spectrometer with a KBr beam splitter and an MCT/A detector under dry air to monitor reaction kinetics at a series scan rate of one scan per 1.8 s. Homogeneous mixtures were sandwiched between NaCl windows with 50 μm plastic spacers and placed into a horizontal transmission apparatus. The conversion of thiol, acrylate, and allyl functional groups was assessed by monitoring the disappearance of peak areas centered around 2570, 810, and 3084 cm^{-1}, respectively.

2.4. Dynamic Mechanical Analysis (DMA). To the homogeneous thiol/acrylate/allyl mixtures containing 0.5 wt % TPO and 0.05 wt % Q1301, 0.5 wt % TEA was added, and then the sample was quickly sandwiched in a glass cell with 1 mm spacers and placed in the dark overnight, forming a stage 1 film resulting from the thiol−Michael reaction. The stage 2 films were prepared by flood curing the stage 1 network by a high-pressure mercury vapor short arc lamp (EXFO Acticure 4000) equipped with a 365 nm short bandpass filter, at an intensity of 20 mW/cm^2 for 10 min on each side. The mechanical characterization of both stage 1 and stage 2 polymer films was performed with a DMA Q800 dynamic mechanical analyzer, where rectangular 10 mm × 5 mm × 1 mm samples were evaluated at a ramp rate of 3 °C/min with a frequency of 1 Hz. The T_g was recorded as the temperature at which the tan δ reached its maximum and rubbery storage moduli were determined at T_g + 30 °C. All samples were tested in triplicate and run twice for each sample.

2.5. Grating Recording and Characterization. To the stoichiometric mixtures of thiol/acrylate/allyl containing 0.5 wt % TPO and 0.05 wt % Q1301, 0.5 wt % TEA was added, and then the sample was quickly sandwiched in a glass cell with 100 μm spacers and placed in the dark overnight, forming a stage 1 film as a result of the thiol−Michael reaction. The holograms were recorded on the stage 1 film by two-beam laser interference at an full angle of approximately 30° with a 405 nm laser at an intensity of 10 mW/cm^2 per beam for 2 s; the graded holograms were recorded on the stage 1 film by two laser beam interference with the help of a cylindrical lens, at an intensity of 10 mW/cm^2 per beam for 5 s (i.e., stage 1 writing step). 4 h later, all holographic films were flood cured by a high-pressure mercury vapor short arc lamp (EXFO Acticure 4000) equipped with a 365 nm bandpass filter, at an intensity of 20 mW/cm^2 for 10 min for each side, forming stage 2 holograms. The rainbow holograms were observed under a fluorescent light. Diffraction efficiency was characterized with a 633 nm red laser, which equaled the ratio of the diffraction intensity to the total intensities for both diffraction and transmission beams. Bulk refractive indices were characterized at 633 nm using a Metricon 2010 prism coupler with a 40 psi air pressure. The data were averaged from five separate samples.

2.6. Atomic Force Microscopy (AFM). Topographical morphologies of the graded rainbow holograms were examined by AFM (Dimension 3100, Vecco) in the tapping mode.

3. RESULTS AND DISCUSSION

A two-stage sequential orthogonal thiol−click approach to form a holographic substrate was implemented, which eliminated the need for solvent processing and/or protective layers to generate holograms but instead afforded good optical clarity, excellent oxygen tolerance, and high light sensitivity for large area hologram production. The two-stage sequential orthogonal thiol−click reactions were implemented using a trithiol trimethylolpropane tris(3-mercaptopropionate) (TMPTMP), a tetraacrylate di(trimethylolpropane)tetraacrylate (DTPTA), a triallyl 1,3,5-triallyl-1,3,5-triazine-2,4,6(1*H*,3*H*,5*H*)-trione (TATATO), and a high refractive index diallyl 9-(2,3-bis(allyloxy)-propyl)carbazole (BAPC) (Scheme 1). The functional group stoichiometric ratio of total thiol to total C═C double bond for all experiments was kept constant at 1:1. The initial part of this study was concentrated on establishing and characterizing the orthogonal nature of thiol−Michael and thiol−allyl radical pathways. Subsequently, the effects varying the allyl to acrylate ratio, and the high refractive index monomer, BAPC, loading

dx.doi.org/10.1021/ma500167x | Macromolecules 2014, 47, 2306−2315

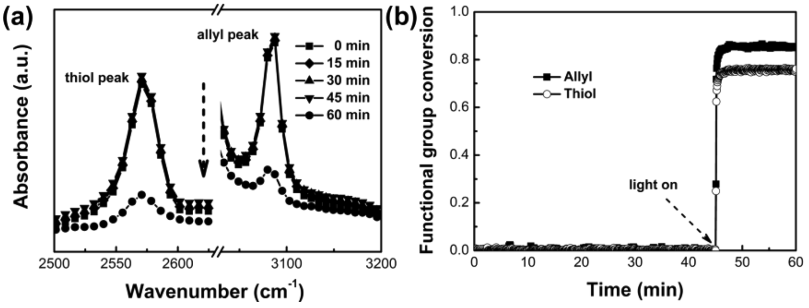

Figure 1. (a) RT-FTIR spectral results and (b) kinetics for the reaction of TMPTMP with TATATO in the presence of the base catalyst TEA. The kinetic results indicate that thiol does not react with allyl monomers through the base-catalyzed Michael addition. The thiol to allyl functional group ratio was 1:1. The homogeneous mixture contained 0.5 wt % TPO and 0.05 wt % Q1301 with 10 wt % TEA. After the kinetics was monitored in the dark for 45 min, the mixture was exposed to 365 nm UV light at an intensity of 20 mW/cm^2 for 15 min.

on the reaction kinetics, mechanics, and diffraction efficiency were assessed.

3.1. TMPTMP/TATATO Thiol−Allyl Reaction in the Presence of Base Catalyst TEA. To verify the orthogonal nature of the thiol−acrylate Michael addition and thiol−allyl radical polymerization, IR spectroscopy was used to monitor the reactions. As shown in Figure 1a, the IR absorption peak of both thiol and allyl does not change in the first 45 min, even when 10 wt % of the base catalyst TEA is added, demonstrating that the thiol−allyl click reaction does not proceed through the thiolate anion pathway. When the light was turned on, however, the thiol−allyl radical photopolymerization proceeded rapidly. Kinetic studies, shown in Figure 1b, clearly illustrate that the thiol−allyl radical photopolymerization is complete in less than 2 min of exposure with 75% of thiol monomer and 86% of allyl monomer converted. The less than 100% of conversion of the thiol monomer is attributed to the decline in mobility resulting from the rapid cross-linking within the network while the 11% higher allyl conversion in comparison to the thiol conversion is attributed to ally homopolymerization which has been previously observed.[42]

3.2. Effect of Allyl to Acrylate Ratio on the Reaction Kinetics, Mechanical Properties, and Holographic Performance. The TMPTMP/DTPTA/TATATO systems with consecutively varied allyl to acrylate ratio are shown in Table 1.

Table 1. Compositions, Stage 2 Allyl Conversion, and Estimated Stage 2 Volume Shrinkage of Networks Formed from Stoichiometric TMPTMP, DTPTA, and TATATO

	total functional group ratio					
entry	TMPTMP	DTPTA	TATATO	allyl to acrylate ratio	stage 2 allyl conv (%)	estd stage 2 volume shrinkage (%)
1	1.3	1.0	0.3	0.3	40	0.7
2	1.7	1.0	0.7	0.7	72	2.2
3	2.1	1.0	1.1	1.1	70	2.8
4	2.5	1.0	1.5	1.5	76	3.5
5	2.9	1.0	1.9	1.9	75	3.8

To demonstrate further the orthogonal nature of the two-stage thiol−vinyl click reactions, we characterized both the Michael addition and photopolymerization kinetics by RT-FTIR. As shown in Figure 2, for the resins with 2.1:1.0:1.1 (thiol:acrylate:allyl) functional group ratio, the thiol−acrylate Michael reaction proceeded when base catalyst TEA was added, but there was no reaction of allyl with thiol during this process.

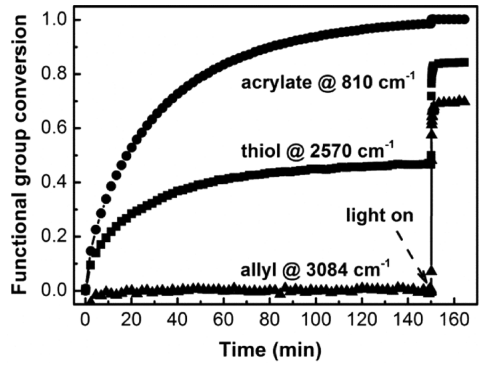

Figure 2. Kinetic curves of thiol (■), acrylate (●), and allyl (▲) in the two-stage orthogonal thiol−click reactions, showing that the thiol−acrylate Michael reaction proceeded in the presence of the base TEA whereas the thiol−allyl reaction was initiated only when the sample was illuminated by light. The homogeneous mixture composed of TMPTMP/DTPTA/TATATO (2.1:1.0:1.1 of functional group ratio), 0.5 wt % TPO, 0.05 wt % Q1301, and 0.5 wt % TEA. After 150 min in the dark, the sample was exposed to 365 nm UV light at an intensity of 20 mW/cm^2 for 15 min.

The acrylate conversion reached 98% while thiol conversion approached 47%, near the expected conversions of 100% and 48%, respectively, for the ideal Michael addition, as calculated from the thiol to acrylate ratio of 2.1:1.0. When the light was turned on, the 2% of unreacted acrylate was converted and yielded 100% acrylate conversion. Meanwhile, the thiol−allyl photoclick reaction proceeded rapidly, being essentially complete after 70 s of light exposure, giving 84% and 70% of thiol and allyl group conversions, respectively. During the photopolymerization, there were 37% the total thiol groups reacted, indicating that 71% the allyl groups should take part in the radical thiol−allyl reaction, in good agreement with the experiment data. When the allyl to acrylate ratio was 0.3, the allyl conversion during the photoinduced reaction was only 40%. The effect of the allyl to acrylate ratio on photopolymeriztion kinetics was also investigated (Figure 3). As the allyl to acrylate ratio rose to 0.7, the allyl conversion increased 1.8 times; however, when further increasing the allyl to acrylate ratio to 1.9, only 76% allyl conversion was observed due to vitrification in the cross-linked networks. As shown in Table 1, when the allyl to acrylate ratio rises from 0.3 to 1.9, we estimate that the photopolymerization volume shrinkage increases from 0.7% to 3.8% according to the shrinkage factor equation[42]

$$VS = [DB]_0 \times DC \times SF \quad (1)$$

dx.doi.org/10.1021/ma500167x | Macromolecules 2014, 47, 2306−2315

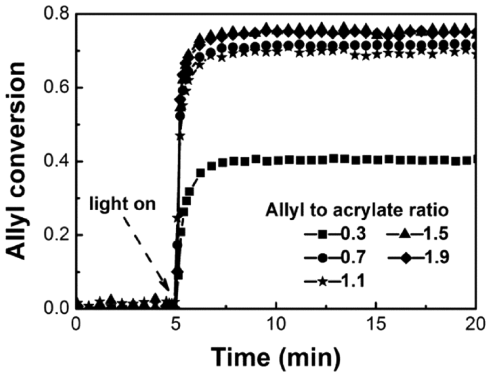

Figure 3. Allyl functional group conversion as a function of allyl to acrylate ratio demonstrating the orthogonal nature of the thiol−Michael and thiol−allyl reactions. Homogeneous mixtures composed of TMPTMP/DTPTA/TATATO with varied functional group ratio and 0.5 wt % TPO, 0.05 wt % Q1301, and 0.5 wt % TEA were sandwiched between NaCl cells with 50 μm spacers and placed in the dark overnight. Subsequently, samples were exposed by 365 nm UV light at the intensity of 20 mW/cm^2 for 15 min, and the reactions were monitored by RT-FTIR.

where VS represents the equilibrium volume shrinkage, $[DB]_0$ and DC are respectively the initial double bond concentration and conversion, and SF is the shrinkage factor and equals 15 mL/mol for the thiol−ene reaction.

Dynamic mechanical analysis (DMA) tests indicate that as the allyl to acrylate ratio increases, the stage 1 rubbery storage modulus decreases from 11.1 to 0.3 MPa while the stage 1 glass transition temperature T_g decreased from 0 to −26 °C (Figure 4). Predictably, the excess thiol and allyl monomers embedded in the stage 1 matrix result in the formation of a more loosely cross-linked network, optimizing monomer diffusion and reaction rates in the thiol−acrylate matrix during the holographic writing step. The cross-link density is calculated based on the rubber elasticity theory in which the rubbery storage modulus is determined at T_g + 30 °C.[49] The stage 1 cross-linking density is reduced from 1.47 to 0.04 M as the allyl to acrylate ratio rises from 0.3 to 1.9. During the flood curing step, excess thiol and allyl monomers are reacted into the polymer network, resulting in a higher stage 2 rubbery modulus and T_g. For instance, during the flood curing, the rubbery modulus and T_g increase by more than 30 times and 40 °C, respectively, when the allyl to acrylate ratio is 1.9.

Diffraction efficiencies at the Bragg angle for the compositions clearly indicate that as the allyl to acrylate ratio grows from 0.3 to 1.1, the diffraction efficiency rises from 0 to 17 ± 2% since monomer diffusion is less hindered in a loosely cross-linked network (Figure 5a). However, when the allyl to acrylate ratio is larger than 1.1, the diffraction efficiency gradually drops to 4 ± 2%, indicating that the index contrast decreases as a result of the bulk refractive index increase from 1.527 to 1.540 (Figure 5b). It was also observed that no holographic grating is generated when the allyl to acrylate ratio is 0.3 though 46% of excess functional groups remain unreacted before photopolymerization and 40% allyl conversion occurs during the stage 2 flood cure. A possible explanation for this observation is that as the unreacted trithiol TMPTMP is tethered within the stage 1 cross-linked network, it cannot freely diffuse from dark region to bright region of interference patterns during holographic writing step, thereby also demonstrating that the thiol−allyl click reaction rather than allyl homopolymerization contributes to the index contrast within the hologram.

3.3. Reaction Kinetics and Mechanical Performances of the Stoichiometric TMPTMP/BAPC System. As the bulk refractive index of the stoichiometric TMPTMP/TATATO film at 633 nm is only 1.557 (0.030 higher than that for the stoichiometric TMPTMP/DTPTA film), to obtain higher diffraction efficiencies, a higher refractive index monomer was synthesized. Chan and co-workers[53] observed that a higher percentage of sulfur incorporated in the network directly resulted in higher refractive indices of polymers. However, as our current systems are based on two-stage thiol−click reactions, an increase in the refractive index of allyl monomers is an effective way to increase the index contrast. Herein, we synthesized a new high refractive index difunctional allyl monomer BAPC. Structural characterization and model reactions of BAPC with the monothiol are given in the Supporting Information.

RT-FTIR experiments were conducted to detect the photoreaction kinetics of stoichiometric BAPC and TMPTMP. As shown in Figure 6, there is no reaction in the first 10 min before the light is turned on, while the conversion for both the thiol and allyl functional groups increases rapidly and reaches a plateau of 93% in 37 s of irradiation, likely limited by vitrification. No homopolymerization of BAPC is observed.

DMA tests show that the network formed from a stoichiometric mixture of TMPTMP and BAPC has a T_g of

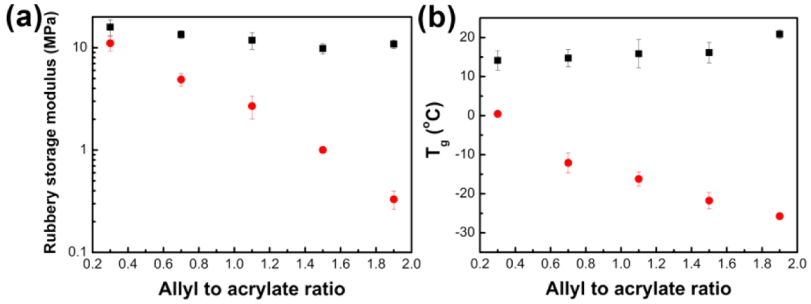

Figure 4. Effect of allyl to acrylate ratio on the (a) rubbery storage modulus and (b) T_g for both stage 1 and stage 2 films formed from stoichiometric TMPTMP/DTPTA/TATATO mixtures. The mixtures containing 0.5 wt % TPO, 0.05 wt % Q1301, and 0.5 wt % TEA were sandwiched in glass cells with 1 mm spacers and placed in the dark overnight, forming stage 1 films. The stage 2 films were prepared by flood curing the stage 1 network under 365 nm UV light at an intensity of 20 mW/cm^2 for 10 min on each side. DMA was performed on a rectangular 10 mm × 5 mm × 1 mm sample over a temperature range of −60 to 60 °C at a ramp rate of 3 °C/min with a frequency of 1 Hz. Rubbery storage moduli were determined at T_g + 30 °C.

dx.doi.org/10.1021/ma500167x | Macromolecules 2014, 47, 2306−2315

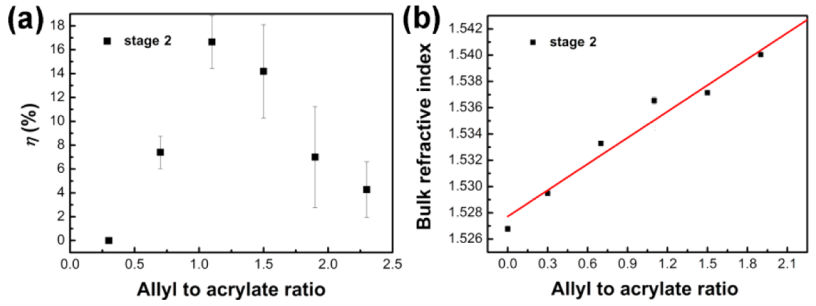

Figure 5. Effect of allyl to acrylate ratio on (a) the stage 2 diffraction efficiency η at the Bragg angle and (b) the bulk refractive index of films formed from a stoichiometric mixture of TMPTMP/DTPTA/TATATO. Figures show that the diffraction efficiency first grows and then decreases with the bulk refractive index rising. Gratings were recorded in 100 μm thick films and then flood cured and characterized at the Bragg angle using a 633 nm laser. Bulk refractive indices were characterized at 633 nm using a Metricon 2010 prism coupler with a 40 psi air pressure.

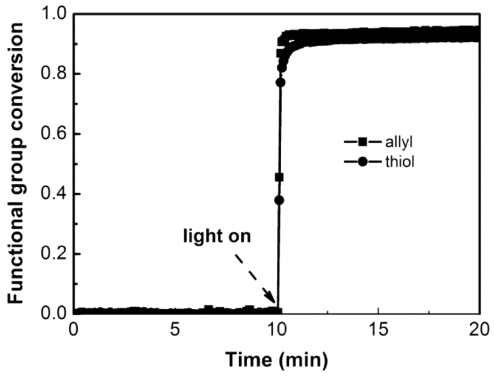

Figure 6. Photoinduced reaction kinetics of TMPTMP with BAPC, showing near-ideal thiol-allyl "click" characteristics. The homogeneous mixture composed of stoichiometric TMPTMP and BAPC, 0.5 wt % TPO, and 0.05 wt % Q1301 was sandwiched in a NaCl cell with 50 μm spacers and placed in the FTIR chamber. After being placed in the dark for 10 min, the sample was exposed by a 365 nm UV light at the intensity of 20 mW/cm^2 for 10 min.

31 °C and a rubbery storage modulus of 4.8 MPa (Figure 7). Prism coupling tests show that the film refractive index at 633 nm is 1.592 (0.065 higher than 1.527 for the TMPTMP/DTPTA film and 0.035 higher than that of the TMPTMP/TATATO film), indicating that the novel monomer BAPC increases the refractive index contrast.

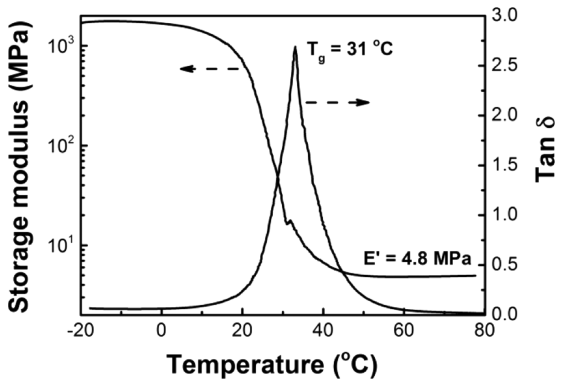

Figure 7. Rubbery storage modulus and T_g for the film formed from stoichiometric TMPTMP and BAPC, showing a narrow glass transition peak. The mixture containing 0.5 wt % TPO and 0.05 wt % Q1301 was sandwiched in a glass cell with 1 mm spacers and flood cured under 365 nm UV light at an intensity of 20 mW/cm^2 for 10 min on each side. DMA was performed on a rectangular 10 mm × 5 mm × 1 mm sample over a temperature range of −20 to 80 °C at a ramp rate of 3 °C/min with a frequency of 1 Hz. Rubbery storage moduli were determined at T_g + 30 °C.

3.4. Effect of BAPC Content on the Holographic Properties. As the composition of 1.1 allyl to acrylate ratio gave the best diffraction efficiency as observed above, the thiol/acrylate/allyl functional group ratio was set as 2.1:1.0:1.1 (thiol:acrylate:allyl) while varying the BAPC and TATATO concentrations (Table 2). As shown in Figure 8a, when the concentration of BAPC rises from 0 to 9 wt %, the diffraction efficiency at the Bragg angle increases from 17 ± 2% to 82 ± 4%; however, it drops to 63 ± 12% when the BAPC content further goes up to 15 wt %. A possible explanation is that incorporating high refractive index BAPC leads to a higher refractive index contrast between the bright and dark region of interference patterns. On the other hand, the index contrast should diminish with higher BAPC loading because of the bulk refractive index increase (Figure 8b), coinciding with the results shown in Figure 5. Another possible reason for the decrease in diffraction efficiency as shown in Figure 8a would be overmodulation effects. However, with an increase in the illumination doses the diffraction efficiency was also seen to increase (not shown here), thereby indicating that the overmodulation effects are negligible.

Table 2. Compositions of Holographic Films with Varied Content of BAPC

total functional group ratio				
TMPTMP	DTPTA	TATATO	BAPC	BAPC content (wt %)
2.1	1.0	1.0	0.1	3
2.1	1.0	0.9	0.2	6
2.1	1.0	0.8	0.3	9
2.1	1.0	0.7	0.4	12
2.1	1.0	0.6	0.5	15

3.5. Orthogonal Reactivity, Mechanical Properties, and Angle-Dependent Diffraction Efficiency for the Composition of TMPTMP/DTPTA/TATATO/BAPC, Where the BAPC Content Is 9 wt %. Figure 9 shows the two-stage orthogonal thiol−allyl reaction curve of the composition containing 9 wt % BAPC. Once the base catalyst TEA was added, the thiol−acrylate Michael addition occurred, and the acrylate conversion reached 100% after 150 min while thiol conversion approached 46%, slightly lower than 48% of the expected conversion. During this thiol−acrylate Michael addition process, no reaction between the thiol with allyl

dx.doi.org/10.1021/ma500167x | Macromolecules 2014, 47, 2306−2315

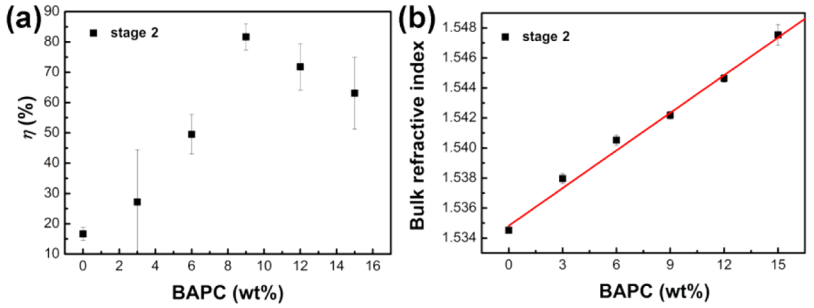

Figure 8. Effect of BAPC content on the (a) stage 2 diffraction efficiency η at the Bragg angle and (b) bulk refractive index of films formed from a stoichiometric mixture of TMPTMP/DTPTA/TATATO/BAPC, showing that the diffraction efficiency increases and then diminishes as the bulk refractive index grows. The initial thiol/acrylate/allyl functional group ratio was 2.1:1.0:1.1 (thiol:acrylate:allyl). Gratings were recorded in 100 μm thick films, then flood cured, and characterized at the Bragg angle using a 633 nm laser. Bulk refractive indices were characterized at 633 nm using a Metricon 2010 prism coupler with a 40 psi air pressure.

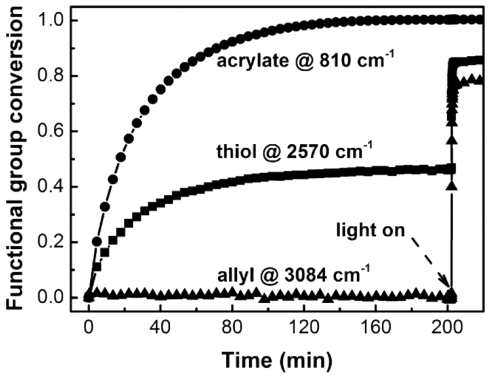

Figure 9. Kinetic curves of thiol (■), acrylate (●), and allyl (▲) in the two-stage orthogonal thiol−click reactions, showing that the thiol−acrylate Michael addition proceeded in the presence of the base catalyst TEA whereas the thiol−allyl radical reaction was initiated only when exposed by light. The homogeneous mixture composed of TMPTMP/DTPTA/TATATO/BAPC (2.1:1.0:0.8:0.3 of functional group ratio), 0.5 wt % TPO, 0.05 wt % Q1301, and 0.5 wt % TEA was sandwiched in a NaCl cell with 50 μm spacers and placed in the IR chamber, after monitoring for 200 min, exposed to 365 nm UV light at an intensity of 20 mW/cm^2 for 20 min.

monomers was observed, demonstrating the orthogonal nature of thiol−Michael and thiol−allyl radical reactions. After the completion of the thiol−acrylate Michael addition, a stage 1 film formed. Subsequent exposure of the stage 1 film for 15 min to a 365 nm light source at an intensity of 20 mW/cm^2 showed that thiol and allyl conversion increased rapidly and leveled off at 85% and 79%, respectively, after 92 s of light exposure. During the photopolymerization, 39% the thiol groups reacted, indicating that 74% the allyl groups should react during this same period. The allyl homopolymerization accounted for the 5% higher conversion obtained from the experiment.[42] From the allyl conversion during stage 2 photopolymerization, a ∼3% photopolymerization volume shrinkage was calculated from the shrinkage factor equation shown in eq 1, which is relatively low for a composition with 51 wt % of unreacted species embedded in the stage 1 matrix. The rapid reaction and relatively low shrinkage are advantageous in forming gratings with high fidelity.

Figure 10 displays the DMA results for the composition with 9 wt % of BAPC. The stage 1 network has a T_g of −14 °C and a rubbery modulus of 3 MPa. After flood curing, the T_g and rubbery storage modulus increase by 30 °C and 1.7 times. On the basis of the rubber elasticity theory, we calculated the cross-linking densities of 0.5 and 1.1 M for stage 1 and stage 2 polymers, respectively, according to the rubbery storage moduli. The bulk refractive index increases at 633 nm from 1.529 for stage 1 to 1.542 after stage 2. Although the cross-linking density increases 2.2 times from stage 1 to stage 2, it is observed that there is only a single T_g peak with peak width at

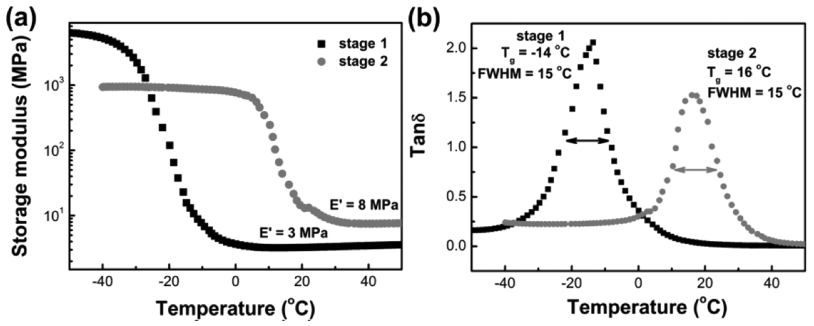

Figure 10. (a) Storage modulus and (b) tan δ as a function of temperature for the stage 1 and stage 2 networks separately formed from a stoichiometric mixture of TMPTMP/DTPTA/TATATO/BAPC (2.1:1.0:0.8:0.3 of functional group ratio), showing that both stage 1 and stage 2 have narrow glass transition peaks and are from similarly homogeneous networks. The mixture containing 0.5 wt % TPO, 0.05 wt % Q1301, and 0.5 wt % TEA were sandwiched in a glass cell with 1 mm spacers and placed in the dark overnight. The stage 2 film was prepared by flood curing the stage 1 network with a 365 nm UV light at an intensity of 20 mW/cm^2 for 10 min on each side. DMA was performed on a rectangular 10 mm × 5 mm × 1 mm sample over a temperature range of −60 to 60 °C at a ramp rate of 3 °C/min with a frequency of 1 Hz. Rubbery storage moduli were determined at the T_g + 30 °C.

dx.doi.org/10.1021/ma500167x | Macromolecules 2014, 47, 2306−2315

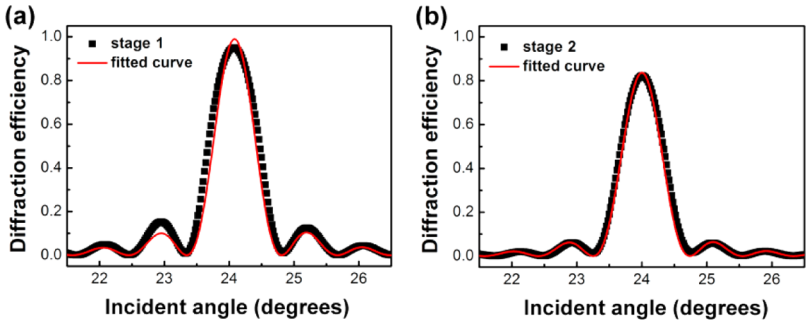

Figure 11. (a) Stage 1 (writing step) and (b) stage 2 diffraction efficiency plots as a function of incident angle showing that the gratings are of good fidelity. The gratings were formed from a stoichiometric mixture of TMPTMP/DTPTA/TATATO/BAPC (2.1:1.0:0.8:0.3 of functional group ratio). The reading beam wavelength = 633 nm.

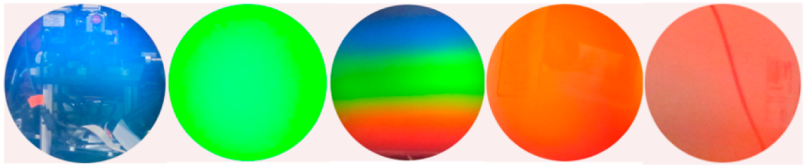

Figure 12. Graded rainbow holograms recorded through a cylindrical technique. The gratings were formed from a stoichiometric mixture of TMPTMP/DTPTA/TATATO/BAPC (2.1:1.0:0.8:0.3 of functional group ratio), and the pattern diameter was 4 mm.

half-height for both stage 1 and stage 2 of 15 °C, implying that the stage 1 and stage 2 polymers both form homogeneous networks without phase separation.

As shown in Figure 11, the diffraction efficiency angle selectivity tests indicate that the stage 1 diffraction efficiency of our gratings composed of TMPTMP/DTPTA/TATATO/BAPC with 9 wt % BAPC was 96 ± 1%. The photosensitivity was calculated as 2.4 cm/mJ (the ratio between the square root of the diffraction efficiency and the product of the film thickness, exposure intensity, and time), which is larger than the typical photosensitivity of 0.5 cm/mJ for photopolymers while remaining well below the photosensitivity level of typical liquid mixtures (6.3 cm/mJ).[4] To achieve a photosensitivity of 2.2 cm/mJ in a photopolymer, Lin and co-workers added 20 wt % of an ionic liquid.[54] Here, no additional additives are needed because a significant amount of excess thiol and allyl monomers are embedded within the network and act as plasticizers to facilitate monomer diffusion until being fully cured during the flood cure, second reaction stage. In addition, the high gel point conversion of the thiol−allyl photopolymerization also accounts for the high light sensitivity because larger amounts of high refractive index monomers can diffuse to the bright region of the interference patterns to increase index contrast before vitrification.

Before flood curing, the increase in the secondary peak of the angle dependent diffraction efficiency curve is indicative of the grating distortion as a result of nonlinear volumetric shrinkage which would be observed even at low shrinkage values such as 0.1%[3] (Figure 11a). For our current system, the distortion is not surprising as the estimated volume shrinkage during the photopolymerization is calculated to be ∼3%. The shrinkage observed is further alleviated by introducing additives such as cyclic allyl sulfides[3] or nanoparticles.[43] After flood curing, the stage 2 diffraction efficiency was reduced to 82 ± 4% as the unreacted monomers in the dark regions were now reacted, thereby diminishing the index contrast. A highly symmetrical, sharp and narrow angle selectivity plot for the stage 2 grating was seen with a bandwidth of 1.5°. From fitting to the Kogelnik's coupled wave theory,[55] we obtain an index modulation of 0.005 and 0.004 for the stage 1 and stage 2 gratings, respectively, while the grating periodicity for both stage 1 and stage 2 is around 780 nm from the fitting. After writing holograms but before the "hardening" step, the films are seen to be "soft" enough to impart mechanically variable diffraction efficiency properties, i.e., one can mechanically squeeze the grating to change the spacing of the fringes. The unique advantage of our material is precisely that we can harden it, which makes it less sensitive to detrimental environmental effects. Therefore, the grating pitches for stage 1 and stage 2 were maintained the same in this study.

3.6. Graded Rainbow Holograms Recording and Display. Graded rainbow holograms are able to show full color at the same viewing angle. Recently, Liu and co-workers developed reflection graded rainbow holograms that displayed full colors at the same viewing angle by using a cylindrical lens, through which multispectral imaging or bioinspired optical applications may be made accessible and affordable.[56] Inspired by this intriguing technique, we fabricated transmission graded rainbow holograms with a continuously variable period. When transmission gratings are patterned through two beam interferences, the grating period Λ_i is determined by the incident angle θ_i of the two beams according to the Bragg condition, $\Lambda_i = \lambda_{writing}/2 \sin(\theta_i/2)$. If the incident beams are introduced from a constant direction, there is only one constant grating period. By contrast, when one coherent beam is introduced from a given incident angle to the lens, its propagation direction expands to several directions that are determined by the beam's spatial location on the curved surfaces of the lens.[56] Consequently, a continuous variation of the incident angle θ_i results, offering a continuously variable grating period Λ_i. Compared to multicolor display of reflection graded rainbow holograms, the transmission graded rainbow holograms show both a single color and multiple colors when the viewer changes the viewing angle.

When viewed under a fluorescent white light from a constant angle ϕ, the peak wavelength λ_i of the diffracted light from

dx.doi.org/10.1021/ma500167x | Macromolecules 2014, 47, 2306−2315

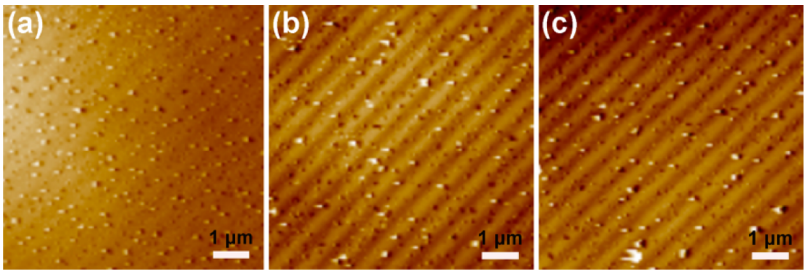

Figure 13. Atomic force microscopy images of the graded rainbow holograms. The grating periods are (a) 867 ± 4, (b) 822 ± 5, and (c) 789 ± 2 nm. The surface height change on the front surface is around 2 nm.

these graded rainbow holograms is given as $\lambda_i = 2\Lambda_i \sin \phi$, indicating that one can inspect several different colors from the same angle. The full color image shown in the middle of Figure 12 confirms that we successfully obtained graded rainbow holograms, and single colors from blue to red are also readily observed. The full color image is an analogue to the logo of TVB, a television channel in Hong Kong. Atomic force microscopy illustrates that the grating period of the graded rainbow holograms changes from 867 ± 4 to 789 ± 2 nm over the exposed area (Figure 13). When we change the white light incident angle and viewer position, the pure colors of blue, green, orange, and red can also result. In comparison, we did not observe multicolor gratings when formed without a cylindrical lens. For the thick films, we expect to observe differences in the grating surface morphology from the front surface to the back surface of the films. However, the differences are seen to relatively small since the surface height change on the front surface is ∼2 nm.

4. CONCLUSIONS

We have successfully demonstrated the formation of graded rainbow holograms that displayed a rainbow of colors at a single viewing angle through a novel strategy of two-stage sequential orthogonal thiol−click polymerization. By carefully and precisely controlling the stoichiometric ratio of the thiol, acylate and allyl present within the network, polymers with a range of glass transition temperatures (T_g) and rubbery storage moduli (E') were designed to optimize monomer diffusion within the network during sequentially orthogonal thiol−allyl "click" photopolymerizations upon holographic illumination. With loading of a novel high refractive index diallyl monomer, holographic gratings were prepared with as high as 96% diffraction efficiency. This unique two-stage sequential orthogonal thiol−click approach eliminates traditional solvent processing and is environmentally friendly; the reactions are also rapid and oxygen tolerant without light scattering or microphase separation, demonstrating good optical transparency and excellent oxygen tolerance. Thus, this work indicates a great potential for two-stage thiol−click chemistry in industrial applications in which the polymer substrates can be designed to have distinct intermediate properties and allow for further processing, consequently afford polymers with tunable ultimate properties.

■ ASSOCIATED CONTENT

Supporting Information

Schemes S1−S2 and Figures S1−S6. This material is available free of charge via the Internet at http://pubs.acs.org.

■ AUTHOR INFORMATION

Corresponding Author

*E-mail: christopher.bowman@colorado.edu (C.N.B.).

Notes

The authors declare no competing financial interest.

■ ACKNOWLEDGMENTS

We appreciate the AFM characterization by Dr. Parag Shah in Prof. Jeffrey W. Stansbury's group and Dr. Sajjad Maruf in Prof. Yifu Ding's group. Useful suggestions were also received from Shunsuke Chatani, Dr. Maciej Podgorski, and Dr. Jiancheng Liu. H.Y. expresses his grateful appreciation for China Scholarship Council award (201206160040). The authors gratefully acknowledge support from the National Science Foundation Grant CHE 1214109.

■ REFERENCES

(1) McLeod, R. R.; Daiber, A. J.; Honda, T.; McDonald, M. E.; Robertson, T. L.; Slagle, T.; Sochava, S. L.; Hesselink, L. *Appl. Opt.* **2008**, *47*, 2696.
(2) Bruder, F.-K.; Hagen, R.; Roelle, T.; Weiser, M.-S.; Faecke, T. *Angew. Chem., Int. Ed.* **2011**, *50*, 4552.
(3) Choi, K.; Chon, J. W. M.; Gu, M.; Malic, N.; Evans, R. A. *Adv. Funct. Mater.* **2009**, *19*, 3560.
(4) Castagna, R.; Vita, F.; Lucchetta, D. E.; Criante, L.; Simoni, F. *Adv. Mater.* **2009**, *21*, 589.
(5) Prime, E. L.; Solomon, D. H. *Angew. Chem., Int. Ed.* **2010**, *49*, 3726.
(6) Blanche, P. A.; Bablumian, A.; Voorakaranam, R.; Christenson, C.; Lin, W.; Gu, T.; Flores, D.; Wang, P.; Hsieh, W. Y.; Kathaperumal, M.; Rachwal, B.; Siddiqui, O.; Thomas, J.; Norwood, R. A.; Yamamoto, M.; Peyghambarian, N. *Nature* **2010**, *468*, 80.
(7) Fattal, D.; Peng, Z.; Tho, T.; Vo, S.; Fiorentino, M.; Brug, J.; Beausoleil, R. G. *Nature* **2013**, *495*, 348.
(8) Smalley, D. E.; Smithwick, Q. Y. J.; V, M. B., Jr.; Barabas, J.; Jolly, S. *Nature* **2013**, *498*, 313.
(9) Ozaki, M.; Kato, J.-i.; Kawata, S. *Science* **2011**, *332*, 218.
(10) Trentler, T. J.; Boyd, J. E.; Colvin, V. L. *Chem. Mater.* **2000**, *12*, 1431.
(11) Setthachayanon, S.; Schnoes, M. US 0044691, 2003.
(12) Nicolas, S.; Friedrich-Karl, B.; Harald, B. US 0062419, 2008.
(13) Khan, A.; Daugaard, A. E.; Bayles, A.; Koga, S.; Miki, Y.; Sato, K.; Enda, J.; Hvilsted, S.; Stucky, G. D.; Hawker, C. J. *Chem. Commun.* **2009**, 425.
(14) Jeong, Y.-C.; Lee, S.; Park, J.-K. *Opt. Express* **2007**, *15*, 1497.
(15) Iha, R. K.; Wooley, K. L.; Nystrom, A. M.; Burke, D. J.; Kade, M. J.; Hawker, C. J. *Chem. Rev.* **2009**, *109*, 5620.
(16) Azagarsamy, M. A.; Anseth, K. S. *ACS Macro Lett.* **2013**, *2*, 5.
(17) Beal, D. M.; Jones, L. H. *Angew. Chem., Int. Ed.* **2012**, *51*, 6320.
(18) Xi, W.; Scott, T. F.; Kloxin, C. J.; Bowman, C. N. *Adv. Funct. Mater.* **2014**, DOI: 10.1002/adfm. 201302847.
(19) Chan, J. W.; Hoyle, C. E.; Lowe, A. B. *J. Am. Chem. Soc.* **2009**, *131*, 5751.

(20) DeForest, C. A.; Polizzotti, B. D.; Anseth, K. S. *Nat. Mater.* **2009**, *8*, 659.
(21) Gupta, N.; Lin, B. F.; Campos, L.; Dimitriou, M. D.; Hikita, S. T.; Treat, N. D.; Tirrell, M. V.; Clegg, D. O.; Kramer, E. J.; Hawker, C. J. *Nat. Chem.* **2010**, *2*, 138.
(22) Yue, K.; Liu, C.; Guo, K.; Yu, X.; Huang, M.; Li, Y.; Wesdemiotis, C.; Cheng, S. Z. D.; Zhang, W.-B. *Macromolecules* **2012**, *45*, 8126.
(23) Kaufmann, T.; Wendeln, C.; Gokmen, M. T.; Rinnen, S.; Becker, M. M.; Arlinghaus, H. F.; Du Prez, F.; Ravoo, B. J. *Chem. Commun.* **2013**, *49*, 63.
(24) Ye, S.; Azarnoush, S.; Smith, I. R.; Cramer, N. B.; Stansbury, J. W.; Bowman, C. N. *Dent. Mater.* **2012**, *28*, 1004.
(25) Barbey, R.; Perrier, S. *ACS Macro Lett.* **2013**, *2*, 366.
(26) Adzima, B. J.; Tao, Y.; Kloxin, C. J.; DeForest, C. A.; Anseth, K. S.; Bowman, C. N. *Nat. Chem.* **2011**, *3*, 256.
(27) Gong, T.; Adzima, B. J.; Baker, N. H.; Bowman, C. N. *Adv. Mater.* **2013**, *25*, 2024.
(28) Orski, S. V.; Poloukhtine, A. A.; Arumugam, S.; Mao, L. D.; Popik, V. V.; Locklin, J. *J. Am. Chem. Soc.* **2010**, *132*, 11024.
(29) Gong, T.; Adzima, B. J.; Bowman, C. N. *Chem. Commun.* **2013**, *49*, 7950.
(30) Wendeln, C.; Singh, I.; Rinnen, S.; Schulz, C.; Arlinghaus, H. F.; Burley, G. A.; Ravoo, B. J. *Chem. Sci.* **2012**, *3*, 2479.
(31) Williams, R. J.; Barker, I. A.; O'Reilly, R. K.; Dove, A. P. *ACS Macro Lett.* **2012**, *1*, 1285.
(32) Zhang, S. Y.; Zou, J.; Zhang, F. W.; Elsabahy, M.; Felder, S. E.; Zhu, J. H.; Pochan, D. J.; Wooley, K. L. *J. Am. Chem. Soc.* **2012**, *134*, 18467.
(33) Shen, Y.; Ma, Y. N.; Li, Z. B. *J. Polym. Sci., Polym. Chem.* **2013**, *51*, 708.
(34) Adzima, B. J.; Kloxin, C. J.; DeForest, C. A.; Anseth, K. S.; Bowman, C. N. *Macromol. Rapid Commun.* **2012**, *33*, 2092.
(35) Saha, A.; De, S.; Stuparu, M. C.; Khan, A. *J. Am. Chem. Soc.* **2012**, *134*, 17291.
(36) Kang, T.; Amir, R. J.; Khan, A.; Ohshimizu, K.; Hunt, J. N.; Sivanandan, K.; Montanez, M. I.; Malkoch, M.; Ueda, M.; Hawker, C. J. *Chem. Commun.* **2010**, *46*, 1556.
(37) Hoyle, C. E.; Bowman, C. N. *Angew. Chem., Int. Ed.* **2010**, *49*, 1540.
(38) Hoyle, C. E.; Lowe, A. B.; Bowman, C. N. *Chem. Soc. Rev.* **2010**, *39*, 1355.
(39) Lowe, A. B.; Hoyle, C. E.; Bowman, C. N. *J. Mater. Chem.* **2010**, *20*, 4745.
(40) Lowe, A. B. *Polym. Chem.* **2010**, *1*, 17.
(41) DeForest, C. A.; Anseth, K. S. *Nat. Chem.* **2011**, *3*, 925.
(42) Lu, H.; Carioscia, J. A.; Stansbury, J. W.; Bowman, C. N. *Dent. Mater.* **2005**, *21*, 1129.
(43) Hata, E.; Tomita, Y. *Opt. Lett.* **2010**, *35*, 396.
(44) Natarajan, L. V.; Shepherd, C. K.; Brandelik, D. M.; Sutherland, R. L.; Chandra, S.; Tondiglia, V. P.; Tomlin, D.; Bunning, T. J. *Chem. Mater.* **2003**, *15*, 2477.
(45) White, T. J.; Natarajan, L. V.; Tondiglia, V. P.; Lloyd, P. F.; Bunning, T. J.; Guymon, C. A. *Polymer* **2007**, *48*, 5979.
(46) White, T. J.; Natarajan, L. V.; Tondiglia, V. P.; Lloyd, P. F.; Bunning, T. J.; Guymon, C. A. *Macromolecules* **2007**, *40*, 1121.
(47) Xi, W.; Krieger, M.; Kloxin, C. J.; Bowman, C. N. *Chem. Commun.* **2013**, *49*, 4504.
(48) Chatani, S.; Nair, D. P.; Bowman, C. N. *Polym. Chem.* **2013**, *4*, 1048.
(49) Xi, W.; Wang, C.; Kloxin, C. J.; Bowman, C. N. *ACS Macro Lett.* **2012**, *1*, 811.
(50) Nair, D. P.; Cramer, N. B.; Gaipa, J. C.; McBride, M. K.; Matherly, E. M.; McLeod, R. R.; Shandas, R.; Bowman, C. N. *Adv. Funct. Mater.* **2012**, *22*, 1502.
(51) Ma, S. J.; Mannino, S. J.; Wagner, N. J.; Kloxin, C. J. *ACS Macro Lett.* **2013**, *2*, 474.
(52) Krevelen, D. W. v.; Nijenhuis, K. T. In *Properties of Polymers*, 4th ed.; Elsevier Science: Amsterdam, 2009; p 290.
(53) Chan, J. W.; Zhou, H.; Hoyle, C. E.; Lowe, A. B. *Chem. Mater.* **2009**, *21*, 1579.
(54) Lin, H. C.; Oliveira, P. W.; Veith, M. *Appl. Phys. Lett.* **2008**, *93*, 141101.
(55) Kogelnik, H. *Bell Syst. Tech. J.* **1969**, *48*, 2909.
(56) Liu, K.; Xu, H.; Hu, H.; Gan, Q.; Cartwright, A. N. *Adv. Mater.* **2012**, *24*, 1604.